

# Absolute abstraction: a renormalisation group approach

Carlo Orientale Caputo\*

SISSA - International School for Advanced Studies, 34136 Trieste, Italy

Elias Seiffert

University of Tübingen, Germany

Enrico Frausin

Università di Trieste, Italy

Matteo Marsili

The Abdus Salam International Centre for Theoretical Physics, 34151 Trieste, Italy

March 4, 2026

## Abstract

Abstraction is the process of extracting the essential features from raw data while ignoring irrelevant details. It is well known that abstraction emerges with depth in neural networks, where deep layers capture abstract characteristics of data by combining lower level features encoded in shallow layers (e.g. edges). Yet we argue that depth alone is not enough to develop truly abstract representations. We advocate that the level of abstraction crucially depends on how broad the training set is. We address the issue within a renormalisation group approach where a representation is expanded to encompass a broader set of data. We take the unique fixed point of this transformation — the Hierarchical Feature Model — as a candidate for a representation which is absolutely abstract. This theoretical picture is tested in numerical experiments based on Deep Belief Networks and auto-encoders trained on data of different breadth. These show that representations in neural networks approach the Hierarchical Feature Model as the data get broader and as depth increases, in agreement with theoretical predictions.

Abstraction refers to the ability to form general concepts from sensory input or raw data. It is well known that representations which are increasingly independent of details arise when raw data is processed in a hierarchy of deeper and deeper layers – both in-silico [1] and in-vivo [2]. Here we argue that universal representations emerge when the

---

\*corienta@sissa.it

process of removing irrelevant details is iterated indefinitely on a universe of data that simultaneously expands in variety, that is when increasing depth is combined with expanding breadth<sup>1</sup>. These universal representations encode the concept of absolute abstraction.

We address this in a minimal setting of unsupervised learning from static data (e.g. images). We shall focus on the internal representation<sup>2</sup> of the data in a deep layer of a learning machine and on how it adapts when the training data expands in scope. This process can be cast within a renormalisation group (RG) framework that allows us to identify the fixed point of the RG transformation with the ultimate outcome of this process when it is repeated indefinitely. The analogy between the process of learning broader and broader data in deeper and deeper layers and the RG in statistical physics [3] (see Fig. 1 A) is based on the observation that higher order features in learning are akin to large scale properties in statistical models, which are those that the RG singles out. This idea is further corroborated by similarities between coarse graining and the evolution of representations with depth [4, 5].

The fact that representations converge to a universal, data-independent, distribution aligns with the Platonic Representation Hypothesis [6], which is receiving more and more empirical support. This states that “Neural networks, trained with different objectives on different data and modalities, are converging to a shared statistical model of reality in their representation spaces” [6]. This hypothesis is consistent with the expectation that a representation encompassing a broader universe of circumstances should be more abstract – i.e. data independent – than one describing only a limited domain. In neural networks, this picture suggests that all data-specific information is transferred to the parameters through which the activity of deep layers propagates to the visible layer. In other words, the fixed point of the RG describes how data is organised in the ideal limit of infinite depth and breadth, irrespective of what the data is about.

Hence this paper approaches the problem of characterising abstract representations on the basis of their sole statistical properties, with no reference to what is being represented, guided only by information-theoretic principles.

When a representation with a fixed capacity is updated to describe data from a broader domain, low level details need to be sacrificed in order to make space for high level features describing the organisation of the data within the broader domain. Fig. 1 C sketches this process for an illustrative example. This process of zooming out to a broader domain while losing low level details can also be inverted, by zooming into a specific part of the data, thus uncovering low level details (see Fig. 1 B). We show that in both cases, the corresponding RG transformation has a unique fixed point which is related to the Hierarchical Feature Model (HFM), recently introduced in [7]. This is reassuring for at least two reasons: First the HFM is a maximum entropy model fully determined by a single sufficient statistics, which is the average level of detail of the features, or the coding

---

<sup>1</sup>We distinguish breadth from width, a term commonly used in the literature to denote the number of variables in different layers.

<sup>2</sup>A representation in this paper is a probability distribution over a set of binary variables.

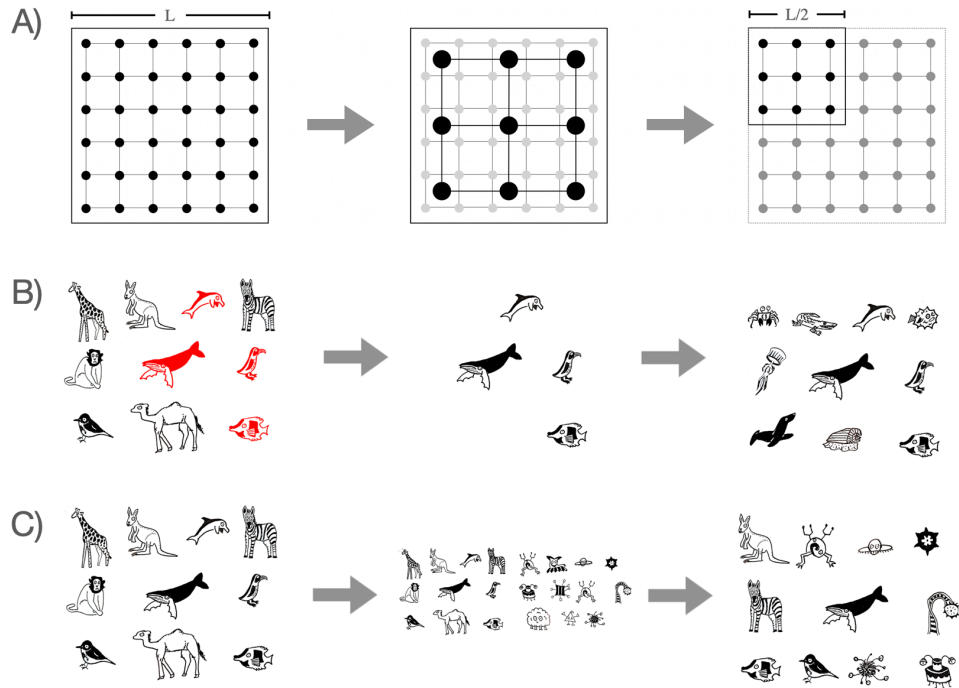


Figure 1: Illustrative example of the RG in statistical physics (A) and of its application in learning (B and C). The RG (A) entails a coarse graining (or decimation) step, whereby low scale degrees of freedom are integrated out, e.g. with the introduction of block variables (large dots in the middle A-panel), and a rescaling step that restores the original size of the system. In a representation of a given domain of items (animals), in B coarse graining is performed zooming into those with a specific feature (living in water) and rescaling corresponds to enriching the representation by adding further details. The same procedure can be reversed (in C): the representation describing a particular domain (animals from planet Earth) is retained on a wider domain (animals from many planets), neglecting small scale details (e.g. the difference between whales and dolphins).

cost. This is indeed the only relevant variable in an abstract representation. Second, the HFM satisfies the principle of maximal relevance<sup>3</sup>, a principle that has been suggested to characterize most informative representations and that also well-trained learning machines have been shown empirically to obey [11, 12].

The rest of the paper is organised as follows: The next Section places our contribution

<sup>3</sup>The relevance has been recently introduced [8] as a quantitative measure of “meaning” that captures Barlow’s intuition [9] that meaning is carried by redundancy. We refer to Appendix A.1 for a brief discussion of the relevance, or to Ref. [10] for an extended account.

within the broader literature on machine learning and neuroscience. Then, in Section 2 we lay out the framework for our analysis. The RG analysis is presented in Section 3. Section 4 discusses numerical experiments on Deep Belief Networks and auto-encoders that corroborate the theoretical predictions. Within their limited expressive capacity, the networks we studied show that representations in deep layers approach the HFM under the combined effects of depth and breadth. Section 5 discusses the results and provides some concluding remarks. All technical details are relegated to the Appendix<sup>4</sup>.

## 1 Literature review

Following Marr [2], we argue that the conceptual underpinnings of the capacity of abstraction are independent of its algorithmic implementation or of whether it is implemented in-silico or in a biological brain. This means that both cognitive neuroscience and machine learning may provide useful insights to characterize abstraction.

Vision provides the paradigmatic case for exploring how abstract representations arise. Both in biological brains [2] and in artificial neural networks (ANNs) [1], vision involves a hierarchical organization of representations: shallow layers detect low-level features, such as edges [14], while deeper layers integrate these features to recognize more abstract, higher-order constructs like objects and faces [1]. In particular, deeper layers are capable of recognising an object or a face irrespective of its position, orientation, scale, or of context<sup>5</sup> [17, 18]. This parallel underscores the broader principle that abstraction emerges through layered processing, regardless of the underlying substrate on which the process is implemented. Yet it has also been argued [19] that the limit of infinite depth is singular, because too much depth without constraints washes away meaningful structure in the input data.

In general, abstract representations extracted from data have been discussed in terms of “cognitive maps” [20, 21]. A cognitive map is not only an efficient and flexible scaffold of data, but it is also endowed with a structure of relations – uncovered from the data – that enables abstract computation<sup>6</sup> [20, 21] and supports complex functions. For example, spatial navigation in rats relies on the representation built by several assemblies of specialised neurons, such as grid cells [22, 23].

At the highest levels of cognition, representations should integrate data from a broad set of domains, or perceptual modalities [24], each of which may be organised according to cognitive maps of a different nature. For example, while visual stimuli are described by

---

<sup>4</sup>The present paper supersedes the preliminary results presented in the Master thesis of one of us [13].

<sup>5</sup>This ability can be promoted in ANN by either augmenting the data using invariances [15] or by explicitly implementing them in their architecture – as in convolutional neural networks [1]. Yet even simple neural networks are able to develop a convolutional structure by themselves [16].

<sup>6</sup>Relational structures such as “Alice is the daughter of Jim” and “Bob is Alice’s brother” allow for computations (e.g. “Jim is Bob’s father”) which are invariant with respect to the context (Alice, Jim and Bob can be replaced by any triplet of persons that stand in the same relation, in this example) [20].

object manifolds with supposedly euclidean topology [25, 26], odours have been suggested to be organised in hyperbolic spaces [27]. Higher order representations that integrate the two should therefore be even more abstract, i.e. independent of the data.

A lot has been understood about the role of depth in learning<sup>7</sup> [25, 28, 29, 26, 30, 31, 32]. In particular, depth exploits the compositional structure of the data boosting training performance [28, 30, 32] and classification capacity [29]. Indeed, inner layers of ANN portray data that correspond to the same object as “object manifolds” [25] that become better and better separable with depth [29], while extracting hierarchies of features that promote taxonomic abstraction<sup>8</sup>. It has been proposed that the superior cognitive abilities of *homo-sapiens* crucially rely on the expansion of the neo-cortex in depth and to specific mutations that supported reliable neural computation [35]. In this respect, our results suggest that exposure to a broad variety of data and stimuli is also essential for the emergence of abstract representations that may support intelligence.

The analogy between the processing of data in deeper and deeper layers and the renormalisation group (RG) in statistical physics [3] has been suggested long ago [4, 5, 36]. This analogy is suggestive because the RG is the theoretical tool to study critical phenomena [3] and both artificial and biological learning exhibit critical features [37, 38, 39, 40, 41, 42]. Koch *et al.* [5] have shown that successive training in deeper layers of neural networks performs an operation similar to coarse graining in the RG. Yet the RG transformation does not only involve coarse graining. It also involves rescaling, which is the operation by which the size of the coarse grained system is restored (see Fig. 1 A). We argue that this ingredient corresponds to a change in breadth, i.e. in the diversity in the input data or stimuli. It is indeed common sense that a representation encompassing a broader universe of circumstances should be more abstract than one describing only a limited domain. Likewise, we argue that representations in higher levels of the cognitive hierarchy, that integrate a broader set of stimuli, should be more abstract, i.e. independent of the data.

The emphasis on a data-independent characterisation of abstraction based only of statistical properties contrasts with the “tuning curve” approach [14, 43], in which levels of abstraction are assessed in terms of the features of the data – e.g. edges or faces – that a representation encodes. Likewise, although we implicitly assume that the representations we are interested in describe structured and learnable data, we shall refrain from assuming any specific data structure like the ones proposed in Refs. [30, 44, 32].

---

<sup>7</sup>Strictly speaking, most of these insights pertain to supervised learning, yet we assume they reveal properties that are relevant also for unsupervised learning, which is our focus.

<sup>8</sup>Taxonomic abstraction is based on the idea that objects are similar if they share the same features (e.g. “cats” and “dogs” both have four legs, a tail, etc) and belong to the same category (mammals). Taxonomic abstraction is fundamentally distinct from thematic abstraction, which is based on co-occurrence between objects that share no features (e.g. “cat” and “sofa”), as discussed in [33]. In deep neural networks [30, 32] shallow layers capture statistical associations (thematic) while deep layers encode compositional, taxonomic structures. A similar transition is observed in humans with development: while children favour thematic abstractions, adults more frequently rely on taxonomic (or categorical) structures [34].

## 2 The framework

In this paper, a representation is a probability distribution  $p(\mathbf{s})$  over the configurations  $\mathbf{s}$  of a hidden layer of a generative neural network, such as a Deep Belief Network (DBN) [45] or an auto-encoders [46]. Hence we focus on unsupervised learning and we assume that the network has been trained on some data  $\hat{\mathbf{x}} = (\mathbf{x}_1, \dots, \mathbf{x}_N)$  of  $N$  data points, with a non-trivial structure. The representation  $p(\mathbf{s})$  is the marginal distribution of activation of variables in the hidden layer induced by the distribution  $p(\mathbf{x})$  of the data, i.e.

$$p(\mathbf{s}) = \sum_{\mathbf{x}} p(\mathbf{s}|\mathbf{x})p(\mathbf{x}). \quad (1)$$

We shall confine our discussion to the case where  $\mathbf{s} = (s_1, \dots, s_n)$  is a string of binary variables  $s_i = 0, 1$ . Otherwise, we shall keep our discussion as general as possible for the time being. More details on network architectures and the data will be given in Section 4 and Appendix C.2, where we shall test our predictions on specific models.

We may think of  $s_i$  as indicator variables of abstract features: i.e.  $s_i = 1$  generates points with feature  $i$  and  $s_i = 0$  does not. In order to keep track of indices, when needed, we shall use the notation  $\mathbf{s}_{1:n} = (s_1, \dots, s_n)$  for the state of the hidden layer, and  $\mathbf{0}$  (or  $\mathbf{0}_{1:n}$ ) to indicate the featureless state, i.e. the one with  $s_i = 0$  for all  $i = 1, \dots, n$ .

## 3 Renormalization transformations

The renormalisation group (RG) [3] translates the process of focusing on large scale properties of statistical models into a mathematical formalism. As shown in Fig 1 A), this process is typically composed of two parts: *i*) coarse graining, whereby small scale details are eliminated and *ii*) rescaling in order to restore the original (length) scale. The combined effect of these two steps is a transformation from a probability distribution  $p(\mathbf{s})$  over the state  $\mathbf{s}$  of the system, to a different one  $p' = \mathfrak{R}[p]$  whose fixed points  $p^* = \mathfrak{R}[p^*]$  describe scale invariant states. Fixed points are endowed with *universal* properties which make them independent of small scale details. In statistical physics,  $p^*$  depends solely on few fundamental characteristics, such as symmetries and conservation laws, space dimension and dimensionality of the relevant variables (order parameters) [3]. In the context of learning, such universal distributions are natural candidates for an abstract representation, and the RG offers the ideal conceptual framework to search for them.

The representation  $p(\mathbf{s})$  of an internal layer of a learning machine depends on its depth but also on the data  $\hat{\mathbf{x}}$  used in training. We focus on how a representation changes when it is trained on a larger dataset  $\hat{\mathbf{x}}' = (\hat{\mathbf{x}}, \hat{\mathbf{x}}_{\text{new}})$  incorporating new data  $\hat{\mathbf{x}}_{\text{new}}$ , thus expanding data's domain (Fig. 1 C), or when the network is trained only on a subset of the data (Fig. 1 B).

### 3.1 Zooming out

We describe how a representation  $p(\mathbf{s})$  defined in terms of  $n$  hierarchical features changes when the data expands to encompass a broader domain. We argue that this transformation entails

- i) to account for large-scale features that were not captured by the initial representation
- ii) to adapt within the limits of finite representational resources and because of this
- iii) to disregard small-scale details<sup>9</sup>.

The representation capacity is limited by the number  $n$  of available features and by the number of bits available to describe a single datapoint, which is measured by the entropy  $H[\mathbf{s}] = -\sum_{\mathbf{s}} p(\mathbf{s}) \log_2 p(\mathbf{s})$ . Within these limits, we assume that representations maximise a notion of informational efficiency. This means that features are used as parsimoniously as possible, and that new data require the introduction of new large scale features which are in no way related to old ones. This reflects the principle that learning should venture into the unknown with no prejudice.

As discussed above, we surmise that this transformation takes place under the combined effects of breadth [i)] and depth [iii)], but since we only focus on the representation  $p(\mathbf{s})$  we will not need to make this explicit. Section 4 will explore how breadth and depth affect the internal representations of specific neural networks and whether the predictions of the theory derived here are supported or not in concrete cases.

Formally, let  $p(\mathbf{s}_{1:n})$  be a representation over  $n$  hierarchical features  $\mathbf{s}_{1:n} = (s_1, \dots, s_n)$  where  $s_1$  is the indicator of the largest scale feature while  $s_n$  relates to details at the smallest scale. We remind that  $s_i$  are binary variables that indicate whether the  $i^{\text{th}}$  feature is present ( $s_i = 1$ ) or not ( $s_i = 0$ ). The transformation  $p \rightarrow p' = \mathfrak{R}_{\uparrow}[p]$  discussed above is realised by the following steps:

1. Add a new random feature with  $p(s_0 = 1) = p(s_0 = 0) = \frac{1}{2}$  [i)], i.e.

$$\tilde{p}(\mathbf{s}_{0:n}) = \frac{1}{2}p(\mathbf{s}_{1:n}) \tag{2}$$

In this step, the representation is expanded to describe a wider universe of objects. The new feature  $s_0$  has a distribution of maximal entropy and it is independent of  $\mathbf{s}_{1:n}$ .

---

<sup>9</sup>It may help to discuss these three steps in a specific example, similar to the one described in Fig. 1 C. Imagine how the representation of animals based on observed species in one continent may have been updated when a different continent was discovered. **i)** An expanded universe of observations may lead to the discovery of a new feature that captures the variability in the broader domain. The geographic location may not be the most efficient way to capture this effect, because there may be species found in both continents or traits that are common across them. Hence **ii)** the set of features used to describe the initial dataset may require an update to describe the broader domain. Finally **iii)** fine grained distinctions (e.g. between species of the same genus) of the initial representation need to be disregarded in order to keep the same representational power.

This captures a genuine discovery process characterised by a large scale organisation (described by  $s_0$ ) which is maximally informative and that cannot be described in terms of combinations of already known features.

2. Shift indices  $\mathbf{s}'_{1:n+1} = \mathbf{s}_{0:n}$  and renormalise

$$p'(\mathbf{s}'_{1:n+1}) = (1 - \alpha)\tilde{p}(\mathbf{s}_{0:n}) + \alpha\delta_{\mathbf{s}'_{1:n+1}, \mathbf{0}_{1:n+1}} \quad (3)$$

where  $\alpha$  should be fixed so that the coding cost  $H[\mathbf{s}_{1:n}] = H[\mathbf{s}'_{1:n}]$  remains the same. This step encodes a reorganisation of features [as in **ii**] consistent with a principle of parsimony in the use of features. Eq. (3) assumes that with this redefinition the featureless state  $\mathbf{s} = \mathbf{0}$  – which corresponds to typical objects that do not require features to be described – is repopulated in order to respect the constraint on the coding cost  $H[\mathbf{s}_{1:n}]$ .

3. Marginalise  $s'_{n+1}$

$$p'(\mathbf{s}'_{1:n}) = \sum_{s_{n+1}=0,1} p'(\mathbf{s}_{1:n+1}). \quad (4)$$

In this step, the most detailed feature is eliminated, analogously to what happens in the coarse graining step of the RG [**iii**].

Without the second step, i.e. with  $\alpha = 0$ , this RG procedure would converge to a distribution  $p(\mathbf{s}) = 2^{-n}$  of independent variables. This, as we shall see, is a possible (although trivial) fixed point with  $H[s_{1:n}] = n$  (in bits). When mixing  $\tilde{p}$  with a deterministic term  $\delta_{\mathbf{s}'_{1:n+1}, \mathbf{0}_{1:n+1}}$ , the coding cost  $H[\mathbf{s}]$  decreases whereas in the other two steps it increases, because the  $n^{\text{th}}$  feature is replaced with a totally random one. Hence there is a unique solution for  $\alpha$  (see Appendix B.1 for more details).

A simple argument shows that the transformation  $p \rightarrow p' = \mathfrak{R}_\uparrow[p]$  converges to a unique fixed point. This is because there is a monotonous relation between  $H[\mathbf{s}]$  and  $\alpha$ . For a fixed  $\alpha$ , the transformation described above is linear, which means that it can be expressed as

$$p'(\mathbf{s}'_{1:n}) = \sum_{\mathbf{s}_{1:n}} p(\mathbf{s}_{1:n}) T_{\mathbf{s}_{1:n}, \mathbf{s}'_{1:n}} \quad (5)$$

where  $\hat{T}$  is a stochastic matrix. The associated Markov chain describes a random walk with resetting [47] on the de Bruijn graph [48], and it is shown in Fig. 2 for  $n = 3$ . This Markov chain is clearly ergodic, because  $\hat{T}^m$  has all strictly positive elements for  $m \geq n$ . This is because each time the variable  $s_0$  is generated at random, so after  $m$  iterations, every state  $\mathbf{s}'_{1:n}$  can be generated. By the theory of Markov chains<sup>10</sup>, under successive

<sup>10</sup>We recall the Perron-Frobenius theorem, which states that a matrix with all positive elements has a unique maximal eigenvalue whose corresponding eigenvector has all positive elements. For an ergodic stochastic matrix this eigenvalue is one and the (left) eigenvector is  $p^*$  in our case.

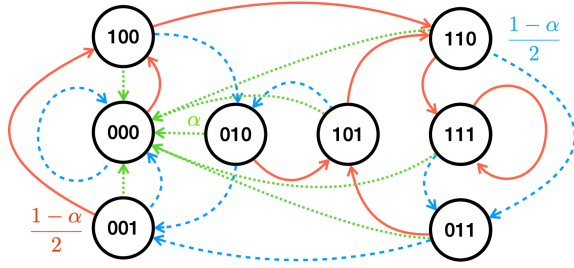


Figure 2: Graphical representation of the transition matrix  $T_{\mathbf{s}_{1:n}, \mathbf{s}'_{1:n}}$  of the coarse graining RG for  $n = 3$ . States are represented by circles and transitions by arrows. From each state  $\mathbf{s}_{1:n}$  there are only three non-zero matrix elements of  $T_{\mathbf{s}_{1:n}, \mathbf{s}'_{1:n}}$ . Two of them correspond to the possible states  $\mathbf{s}'_{1:n} = (s_0, \mathbf{s}_{1:n-1})$  that can be reached by either adding  $s_0 = 1$  to the left of  $\mathbf{s}_{1:n}$  (red links) or adding  $s_0 = 0$  (blue dashed links). Both transitions occur with probability  $T_{\mathbf{s}_{1:n}, \mathbf{s}'_{1:n}} = \frac{1-\alpha}{2}$ . The third transition resets to the  $\mathbf{0}_{1:n}$  state (green dotted links) and it occurs with probability  $T_{\mathbf{s}_{1:n}, \mathbf{0}_{1:n}} = \alpha$ .

applications of the transformation, the distribution converges to a fixed point  $p^*$  from any initial distribution  $p$ , and the limit is unique. The same necessarily applies to the transformation where  $H[\mathbf{s}]$  is held fixed.

The unique fixed point  $p^*$  of the RG transformation, in terms of the parameter  $\alpha \in [0, 1]$ , is given by (see Appendix B.2)

$$p^*(\mathbf{s}) = \frac{2\alpha}{1+\alpha} \left( \frac{1-\alpha}{2} \right)^{m_{\mathbf{s}}} + \frac{1-\alpha}{1+\alpha} \left( \frac{1-\alpha}{2} \right)^n \quad (6)$$

where

$$m_{\mathbf{s}} = \max\{i : s_i = 1\}, \quad (\mathbf{s} \neq \mathbf{0}) \quad (7)$$

is the index of the most detailed active feature in  $\mathbf{s}$ , that we shall call the *level of detail*, and  $m_{\mathbf{0}} = 0$ . Interestingly, this distribution is related to the Hierarchical Feature model (HFM), introduced recently in Ref. [7], which is defined as

$$h_n(\mathbf{s}) = \frac{1}{Z_n} e^{-gm_{\mathbf{s}}}, \quad Z_n = 1 + \frac{1 - (2e^{-g})^n}{e^g - 2}, \quad (8)$$

where  $g \geq 0$  is a parameter (see Appendix A.2 for a discussion of the HFM).

Indeed, with  $\alpha = 1 - 2e^{-g}$  one can show (see Appendix B.2) that  $p^*$  coincides with the marginal distribution of the  $n$  most coarse grained features of an HFM with infinite features:

$$p^*(s_{1:n}) = \lim_{m \rightarrow \infty} \sum_{s_{n+1:m}} h_m(s_{1:m}). \quad (9)$$

We shall come back to the significance of this result after discussing an analogous transformation that proceeds in the opposite direction, describing how a representation changes when zooming into a part of the dataset.

### 3.2 Zooming in

The inverse transformation  $\mathfrak{R}_\downarrow$  to the one described above, describes how the internal representation of a learning machine changes, in ideal circumstances, when we focus on a specific subclass of objects while enriching the data of further small scale details. Again we shall require that the coding cost  $H[\mathbf{s}]$  of the representation remains constant in this process. The same general arguments as those discussed above for  $\mathfrak{R}_\uparrow$  apply. The fine graining transformation  $p \rightarrow p' = \mathfrak{R}_\downarrow[p]$  is based on the following steps.

1. Zooming in on objects with  $s_1 = 1$

$$p(\mathbf{s}_{2:n}) = p(\mathbf{s}_{2:n}|s_1 = 1) \quad (10)$$

2. Shift indices  $\mathbf{s}'_{1:n-1} = \mathbf{s}_{2:n}$  and define  $\tilde{p}(\mathbf{s}'_{1:n-1}) = p(\mathbf{s}_{2:n})$ .

3. Add a new feature  $s'_n$

$$p'(\mathbf{s}'_{1:n}) = p'(\mathbf{s}'_{1:n-1}|s'_n) p(s'_n) \quad (11)$$

where  $p(s'_n = 1) = q = 1 - p(s'_n = 0)$  is determined by requiring that the new representation has the same coding cost as the old one, i.e.  $H[\mathbf{s}'_{1:n}] = H[\mathbf{s}_{1:n}]$ . Also we assume

$$p'(\mathbf{s}'_{1:n-1}|s'_n = 0) = \tilde{p}(\mathbf{s}'_{1:n-1}) \quad (12)$$

$$p'(\mathbf{s}'_{1:n-1}|s'_n = 1) = 2^{-n+1}. \quad (13)$$

The first of these two equations implies that the representation without the new feature is the same as the original representation over  $\mathbf{s}_{2:n}$ . The second equation enforces a maximum ignorance principle whereby the presence of the  $n^{\text{th}}$  feature ( $s_n = 1$ ) does not provide any information on whether more coarse grained features are present or not. This is the equivalent of the first step of the procedure of Sect. 3.1, where higher order features are introduced independently of lower order ones. Indeed, by Eq. (2),  $p'(s'_1|\mathbf{s}'_{2:n} \neq \mathbf{0}_{2:n}) = p(s'_1) = \frac{1}{2}$ .

We can appeal to the same arguments as in Section 3.1 to show that the transformation  $p \rightarrow p' = \mathfrak{R}_\downarrow[p]$  has a unique fixed point<sup>11</sup>. It is also easy to check that the fixed point is

<sup>11</sup>The transformation  $p \rightarrow p' = \mathfrak{R}_\downarrow[p]$  is given by  $p'(\mathbf{s}'_{1:n}) = \frac{q}{2^n} \delta_{s'_n,1} + (1-q)p(\mathbf{s}_{2:n}|s_1 = 1)\delta_{s'_n,0}$ . Strictly speaking, this is not a linear transformation because of the conditional probability  $p(\mathbf{s}_{2:n}|s_1 = 1)$  that appears in the right hand side. Yet it satisfies all the conditions of the non-linear Peron-Frobenius theorem [49] that leads to the same conclusions of the existence of a unique fixed point  $p^* = \mathfrak{R}_\downarrow[p^*]$ . In particular any state  $\mathbf{s}'$  can be reached with finite probability from any other state  $\mathbf{s}$  in a finite number of steps (irreducibility and primitivity).

the HFM, i.e.

$$p^*(\mathbf{s}_{1:n}) = h_n(\mathbf{s}_{1:n}), \quad (14)$$

with a value of  $g$  that depends on  $H[\mathbf{s}]$  (or  $q$ ). Indeed if Eq. (14) holds, then Eq. (12) is satisfied because  $p^*(\mathbf{s}_{2:n}|s_1 = 1) = h_{n-1}(\mathbf{s}_{2:n}) = p^*(\mathbf{s}_{1,n-1}|s_n = 0)$  and the HFM satisfies the condition (13) by definition.

### 3.3 Significance of the results

The fact that the fixed point of the RG transformation is related to the HFM is interesting. Let us discuss the different aspects:

**Data-independence of the internal representation** If the internal representation  $p(\mathbf{s})$  approaches a universal distribution with depth and breadth, then  $p(\mathbf{s})$  does not contain any information on the specific nature of the data that it represents. Data specific information is stored in the conditional distribution  $p(\mathbf{x}|\mathbf{s})$  that generates data points  $\mathbf{x}$  from a given internal state  $\mathbf{s}$ . The internal representation  $p(\mathbf{s})$  captures merely the way in which data is organised into combinations of features that are reproduced by the parameters learned by each layer combining the features learned by the earlier layer. Ref. [7] argues that an architecture where  $p(\mathbf{s})$  is held fixed provides advantages which make learning more similar to understanding.

**Level of detail as sufficient statistics** The HFM was introduced in [7] as an efficient scaffold for data based on two principles. First, the HFM assumes that features are organised in a hierarchical scale of detail and it requires that the occurrence of a feature  $s_k = 1$  at level  $k$  does not provide any information on whether lower order features are present or not. This means that, conditional on  $s_k = 1$ , all lower order features are as random as possible, i.e.  $H[\mathbf{s}_{1:k-1}|s_k = 1] = k - 1$  in bits. This requirement implies that the distribution  $p(\mathbf{s})$  should be a function of  $m_{\mathbf{s}}$ , as defined in Eq. (7), i.e. of the level of detail of objects associated to state  $\mathbf{s}$ . This is equivalent to requiring that the level of detail  $m_{\mathbf{s}}$  is the only sufficient statistics of the distribution, in the sense that knowledge of the probability  $p(m_{\mathbf{s}} = k)$  is sufficient to specify the full distribution  $p(\mathbf{s})$ . If one further requires that just the average level of detail  $\bar{m} = \langle m_{\mathbf{s}} \rangle$  is sufficient to determine  $p(\mathbf{s})$ , i.e. that  $p(\mathbf{s})$  is a maximum entropy distribution, then this implies that the dependence of  $p(\mathbf{s})$  on  $m_{\mathbf{s}}$  should take an exponential form, which singles out Eq. (8) as the only possible solution.

**Relation with the principle of maximal relevance** The maximum entropy requirement also coincides with demanding that  $p(\mathbf{s})$  satisfies the principle of maximal relevance. The relevance is defined [10] as the entropy  $H[E]$  of the coding cost  $E_{\mathbf{s}} = -\log p(\mathbf{s})$  and is discussed in further detail in Appendix A.1. For our discussion, let it suffice to say that

the relevance is a model-free measure of “meaningful” information content in a representation or in a data-set. Indeed, the internal representation of learning machines trained on non-trivial real data approach closely distributions of maximal relevance [11, 12, 10]. The principle of maximal relevance predicts that the number of states  $\mathbf{s}$  with coding cost equal to  $E$  should increase exponentially in  $E$ , i.e.  $W(E) = W_0 e^{\nu E}$  [40, 10]. The HFM satisfies this property with  $\nu = \log 2$  because the number of states with  $m_{\mathbf{s}} = k$  equals  $2^{k-1}$  ( $k > 0$ ). Linearity of  $E_{\mathbf{s}}$  with  $m_{\mathbf{s}}$  implies that the number of bits required to describe a state  $\mathbf{s}$  increases linearly with its level of detail.

### Statistical mechanics of the HFM and the thermodynamics of thought process

In the limit  $n \rightarrow \infty$  the HFM features a phase transition at  $g_c = \log 2$  between a random phase where the entropy  $H[\mathbf{s}]$  and the average number of features  $\langle m_{\mathbf{s}} \rangle$  are of order  $n$  for  $g < g_c$ , and a “low temperature” phase where  $h_n(\mathbf{s})$  is dominated by a finite number of states, with  $H[\mathbf{s}]$  and  $\langle m_{\mathbf{s}} \rangle$  attaining finite limits as  $n \rightarrow \infty$ . The distribution  $h_n(\mathbf{s})$  for  $g = g_c$  reproduces Zipf’s law, a statistical regularity that characterises many efficient representations, from language [50], to assemblies of neurons [39] and the immune system [51]. We refer to [7] for further discussion of the properties of the HFM.

The HFM is particularly intriguing for the peculiarity of its free energy landscape. The fact that the number of states  $W(E)$  at energy  $E$  grows exponentially with  $E$  implies that the entropy  $S(E) = k_B \log W(E)$  is linear in  $E$ . This means that also the free energy  $F(E) = E - TS(E)$  is linear in  $E$  and that there is a temperature for which  $F(E) = F_0$  is constant. At this temperature, transitions from states of different energy require no work, in principle. These transitions, where either more details are added (increasing the level of detail  $E$ ) or removed (decreasing  $E$ ), are the natural building blocks of thought processes like generalization or specialization.

**Marginalization properties of the HFM** For  $g \leq g_c$  the constant  $\alpha = 1 - 2e^{-g}$  in the distribution  $p^*$  of Eq. (6) becomes negative. So the marginal HFM Eq. (9) describes the fixed point of the transformation where the universe of the data expands only for  $g \geq g_c$ . Indeed, marginalising over the high order features yields a mixture between the HFM and the uniform (maximum entropy) distribution (see Appendix B.2)

$$\sum_{\mathbf{s}_{n+1:m}} h_m(\mathbf{s}_{1:m}) = \frac{Z_n}{Z_m} h_n(\mathbf{s}_{1:n}) + \left(1 - \frac{Z_n}{Z_m}\right) 2^{-n}. \quad (15)$$

Eq. (6) coincides with the limit  $m \rightarrow \infty$  of this expression, which returns the uniform distribution  $p(\mathbf{s}) = 2^{-n}$  when  $g \leq g_c$ . This corresponds to the degenerate limit when  $H[\mathbf{s}] = n$  (in bits). For all values  $H[\mathbf{s}] < n$  the fixed point has  $g > g_c$ .

On the other hand, marginalising  $h_n(\mathbf{s}_{1:n})$  over the low order features  $\mathbf{s}_{1:k}$  returns a

mixture between a HFM over the remaining  $n - k$  features and the featureless state

$$\sum_{\mathbf{s}_{1:k}} h_n(\mathbf{s}_{1:n}) = \frac{\xi^k Z_{n-k}}{Z_n} h_{n-k}(\mathbf{s}_{k+1:n}) + \frac{(1 - \xi/2)(\xi^k - 1)}{(\xi - 1)Z_n} \delta_{\mathbf{s}_{k+1:n}, \mathbf{0}_{k+1:n}}, \quad (16)$$

where  $\xi = 2e^{-g}$ . Marginalising over an infinite number of low order features yields

$$\lim_{k \rightarrow \infty} \sum_{\mathbf{s}_{-k+1:n}} h_{n+k}(\mathbf{s}_{-k+1:n}) = \begin{cases} \delta_{\mathbf{s}_{1:n}, \mathbf{0}_{1:n}} & \text{if } g \geq g_c \\ (1 - a) h_n(\mathbf{s}_{1:n}) + a \delta_{\mathbf{s}_{1:n}, \mathbf{0}_{1:n}} & \text{if } g < g_c \end{cases} \quad (17)$$

with  $a = (2\xi - 1)\xi^{-n}$ . Therefore integrating out low or high order features leads to degenerate distributions – either the one concentrated on the featureless state or the totally random one. This is consistent with the fact that coarse graining alone is not sufficient to define a RG. New information has to be injected at each RG step.

## 4 Empirical evidence in Deep Neural Networks

In this Section we test the ideas discussed in previous Sections on two architectures, Deep Belief Networks (DBNs) and auto-encoders (AE), trained on different datasets which are variants of the MNIST dataset of handwritten digits. A full account of architectures, algorithms and datasets is given in Appendix C. We retain the essential details in what follows.

### 4.1 Comparing internal representations with the HFM

As a measure of the distance of representations to the HFM we take the Kullback-Leibler (KL) divergence between the empirical distribution of internal layers and the HFM. The empirical distribution is obtained either as the distribution of clamped states, i.e. of states obtained propagating each datapoint through the layers of the network, or sampling the distribution by Montecarlo methods.

We first observe that the  $n$  hidden binary variables  $\mathbf{s}$  of the internal representation may not coincide with the variables  $\mathbf{s}'$  that appear in the HFM. Thus it is necessary to define the transformation  $\mathbf{s} \rightarrow \mathbf{s}'$ .

First note that the two values  $s_i = 0$  or  $1$  of each variable can be associated in two different ways to the values of  $s'_i$ . Hence a state  $\mathbf{s}$  defined by  $n$  hidden binary variables, admits  $2^n$  possible states  $\mathbf{s}'$ , each consistent with the “gauge”  $\tau$  that defines the transformation  $s_i \rightarrow s'_i = \tau_i s_i + (1 - \tau_i)(1 - s_i)$  with  $\tau_i = 0, 1$ . In order to fix this gauge we set  $\tau$  such that the most frequently sampled state in each representation corresponds to the featureless state  $\mathbf{s}' = \mathbf{0}$ , as for the HFM. In addition, while in the neural networks the variables  $s_i$  are *a priori* equivalent, in the HFM they are not, because they are hierarchically organised. There are  $n!$  possible ways to order the variables  $\mathbf{s}'_{1:n}$ , that correspond to a different HFM.

For a given permutation  $\pi = (\pi(1), \dots, \pi(n))$  of the integers  $1, \dots, n$ , and a given gauge  $\tau$ , the combined effect of these two operations defines the transformation

$$\mathbf{s}' = \mathcal{G}_{\tau, \pi}(\mathbf{s}), \quad s'_i = \tau_{\pi(i)} s_{\pi(i)} + (1 - \tau_{\pi(i)})(1 - s_{\pi(i)}). \quad (18)$$

The transformation  $\mathbf{s} \rightarrow \mathbf{s}'$  that is used to compare internal representations of neural networks with the HFM is obtained minimizing their KL divergence

$$\mathbf{s} \rightarrow \mathbf{s}' = \arg \min_{\pi, g} D_{KL} [\hat{p}(\mathbf{s}) \| h_n(\mathcal{G}_{\tau, \pi}(\mathbf{s}))], \quad (19)$$

where the minimum is taken over all permutations and on the parameter  $g$  of the HFM. In practice, the minimum over permutations is carried out by a greedy heuristics that compares two permutations that differ by the swap of two indices. We consider all possible swaps of indices recursively until no improvement is possible. All results of this Section are derived performing this transformation.

## 4.2 Deep Belief Networks

Deep Belief Networks (DBNs) are layered networks composed of stacked Restricted Boltzmann Machines (RBMs), whereby the hidden layer of one RBM coincides with the visible layer of the deeper RBM. The  $\ell^{\text{th}}$  hidden layer, which is the hidden layer of the  $\ell^{\text{th}}$  RBM, contains  $n_\ell$  binary variables  $\mathbf{s}_\ell \in \{0, 1\}^{n_\ell}$ .

We trained DBNs on datasets of increasing breadth by successively training the RBMs that connect its layers [45]. Starting from the data  $\hat{\mathbf{x}} \equiv \hat{\mathbf{s}}^{(0)}$ , we train layer  $\ell = 1, 2, \dots, L$  from the dataset  $\hat{\mathbf{s}}^{(\ell-a)}$  by maximising the likelihood

$$\mathcal{L}_\ell(\theta_\ell) = \sum_{\mathbf{s}_{\ell-1}} \hat{p}(\mathbf{s}_{\ell-1}) \log \sum_{\mathbf{s}_\ell} p(\mathbf{s}_{\ell-1}, \mathbf{s}_\ell | \theta_\ell) \quad (20)$$

over the parameters  $\theta_\ell$  of the joint distribution  $p(\mathbf{s}_{\ell-1}, \mathbf{s}_\ell | \theta_\ell)$ . The architecture used is the same as that used in Ref. [11] with ten layers of width  $n_\ell = 500, 250, 120, 60, 30, 25, 20, 25, 10$  and 5 for  $\ell = 1, 2, \dots, 10$ . For each trained network we make sure that it correctly generates data-points that are statistically similar to those in the dataset, avoiding known pathologies of these networks [45]. We discuss more details on the architecture, datasets and training algorithms in Appendix C.2. Here we focus on the results.

The results of extensive numerical experiments on DBNs are presented in Fig. 3, which displays the Kullback-Leibler divergence per node<sup>12</sup>  $D_{KL}(\hat{p}_\ell \| h_{n_\ell})/n_\ell$  in colour code (see bar on the left) as a function of breadth and depth (for layers<sup>13</sup>  $\ell = 5$  to 9). We found that  $D_{KL}(\hat{p}_\ell \| h_{n_\ell})/n_\ell$  generally decreases when both depth and breadth increase, as suggested

<sup>12</sup>In the DBN we studied the number of hidden nodes  $n_\ell$  vary substantially with depth  $\ell$ . We expect  $D_{KL}(\hat{p}_\ell \| h_{n_\ell})$  to be proportional to  $n_\ell$ , which is why we show the Kullback-Leibler divergence per node.

<sup>13</sup>We could not reliably estimate the distribution  $p(\mathbf{s})$  for shallower layers.

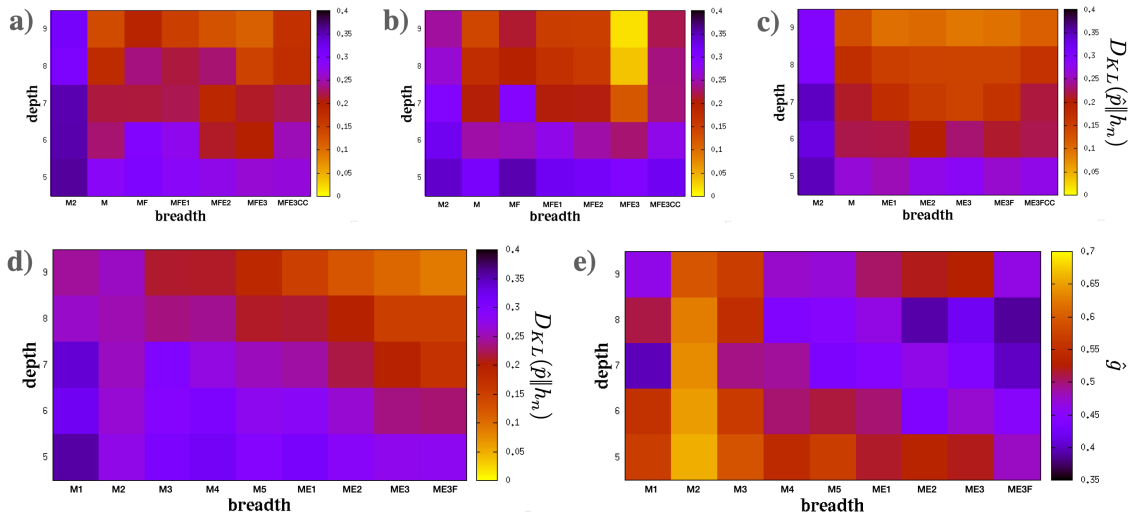


Figure 3: Color plot of the  $D_{KL}$  divergence per node between the internal representation of a layer inside a DBN and the HFM (**a**, **b**, **c** and **d**) and of the fitted parameter  $g$  (**e**) for the DBN in panel **d**). The internal representation is obtained sampling  $10^5$  configurations  $\mathbf{s}$  for each layer from the equilibrium distribution. The DBN’s are trained on datasets of increasing breadth: in **a**), **b**) and **c**) M2 refers to a dataset obtained by transforming the digits 2 of MNIST with translations and rotations, to obtain  $N = 6 \cdot 10^4$  data points, and M refers to the complete MNIST dataset. In **a**) and **b**) MF refers to MNIST plus Fashion MNIST, MFE1 coincides with MF plus the letters from  $a$  to  $i$  of EMNIST, adding letters up to  $r$  generates MFE2 and adding all letters yields MFE3. MFE3CC contains all the data of MFE3 plus Cifar-10 images, rescaled to  $28 \times 28$  pixels. The DBNs in **a**) and **b**) are trained for  $10^5$  and  $10^4$  epochs respectively. DBNs in **c**) and **d**) are also trained for  $10^5$  epochs. In **c**) the order with which the data sets are learned is changed: After MNIST the DBN is trained first with letters in EMNIST and then with images of Fashion MNIST and finally Cifar-10 is added (ME3FCC). In **d**) the datasets are fragmented in different ways. First MNIST is divided into 5 parts (M1 with digits 0 and 1, M2 up to 3, M3 up to 5, M4 up to 7 and M5 with all digits) then EMNIST and Fashion MNIST are added as before. For this network, the fitted value of the parameter  $g$  of the HFM is shown in panel **e**).

by the RG approach. For a fixed depth, the internal representation initially approaches the HFM as breadth increases and subsequently diverges from it. This suggests that both depth and breadth are necessary for abstraction to emerge, as claimed in the theoretical analysis of the previous Section.

Fig. 3 suggests that this conclusion is robust with respect to varying the training time, the order in which datasets are learned and how they are segmented. Specifically, panels **a**) and **b**) compare the same DBN trained for  $10^5$  (**a**) or  $10^4$  (**b**) epochs. We found evidence

that convergence to stable distributions requires long training times, as observed by Decelle and co-workers [52]. Consistently, we found that, although the approach to the HFM is observed in both cases, the convergence is smoother for longer training times (**a**) than for shorter times (**b**)<sup>14</sup>. Panels **a**) and **c**) compare the same DBNs trained (for  $10^5$  epochs) on the same datasets learned in a different order: in **a**) Fashion MNIST is introduced before EMNIST while in **c**) we did the opposite. This comparison shows that, although both cases qualitatively agree with our thesis, the order in which datasets are learned matters: adding datasets which are more similar to those already learned results in a smoother approach to the HFM. The comparison between panels **c**) and **d**) – where the MNIST dataset is disaggregated in 5 parts which are added sequentially – further corroborates this conclusion<sup>15</sup>. Panel **e**) shows that the fitted values of the parameter  $g$  of the HFM decrease with breadth. This is consistent with the fact that in order to represent a wider universe of data, the internal representation needs to expand (indeed the entropy  $H[\mathbf{s}]$  is a decreasing function of  $g$ ). Results obtained fitting the marginal HFM (Eq. 9) lead to similar conclusions.

### 4.3 Auto-encoders

An auto-encoder (AE) is a neural network based on two main components: an encoder, which maps input data to a lower-dimensional latent space, and a decoder, which reconstructs the original data from this latent representation. Both the encoder and the decoder are neural networks of  $L \geq 1$  layers, which are jointly trained to minimize reconstruction error. We trained AE of different depth  $L$  on different datasets, keeping a fixed number  $n$  of variables in the latent representation. We refer to Appendix C.3 for further details on the architectures used.

AEs are deterministic neural networks based on real valued variables. In order to express the latent representation in terms of binary variables, we adopt a sigmoid transfer function between the last layer of the encoder and the latent space, so that latent variables can be interpreted as probabilities from which we sample binary variables. We construct an empirical distribution  $\hat{p}(\mathbf{s})$  by sampling ten states  $\mathbf{s} \in \{0, 1\}^n$  from the activity patterns generated by each point in the dataset. This is then analysed with the same method described in Section 4.1 in order to compute the Kullback-Leibler divergence to the HFM.

Fig. 4 **a**) shows the network architectures used in this study. These are designed so that the AE with  $L + 1$  hidden layers is obtained from that with  $L$  layers adding a further layer between the last and the bottleneck, for both the encoder and the decoder. This procedure is meant to mimic the addition of a further coarse graining step in the

---

<sup>14</sup>Increasing further the training time (to  $10^6$  epochs) led to the collapse of representations to distributions sharply peaked on one or two states.

<sup>15</sup>In the DBNs in **d**) the addition of the Cifar-10 dataset to ME3F (see caption) led to the collapse of the representation (which is why it was not shown). This is a manifestation of the limits of the representation capacity of these neural networks [53].

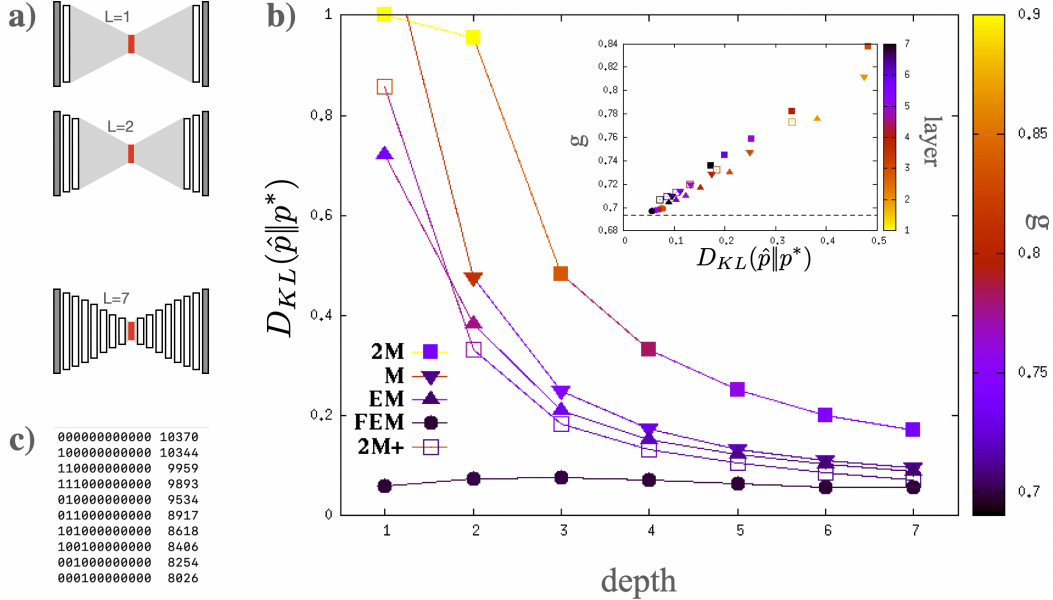


Figure 4: **a)** Architectures of the AE used in this study. The hidden layers (white sticks) process information from the visible layer of the encoder (in grey, left) to the bottleneck layer (in red), which is then propagated through a specular sequence of hidden layers to the visible layer of the decoder (in grey). The architecture with  $L + 1$  layers is obtained adding an extra hidden layer between the last one of the AE with  $L$  layers, on both sides of the bottleneck. **b)** Kullback-Leibler divergence from the marginal HFM  $p^*$  of Eq. (9) of the latent representation of AEs with  $n = 12$  latent nodes and different depths. Each curve refers to a different dataset: 2M contains the point corresponding to digits 2 of MNIST, 2M+ is derived from 2M adding data points obtained through translations and rotations of the original data points. M is MNIST, EM is EMNIST and FEM includes EMNIST and Fashion MNIST. The colour code of points corresponds to the fitted value of  $g$ . The inset reports the values of  $g$  as a function of the Kullback-Leibler divergence, for different layers rendered by the colour code (same symbols as in the main figure). **c)** List of the ten most probable configurations of the latent space with their frequency for the AE with 6 hidden layers trained on the FEM dataset.

information processing before the bottleneck<sup>16</sup>. With increasing depth and expanding breadth, we expect that the latent representation approaches  $p^*$  of Eq. (9).

Fig. 4 **b)** corroborates this expectation. It reports the Kullback-Leibler divergence

<sup>16</sup>The data in Fig. 4 **b,c)** correspond to averages over 6 AE trained from scratch from a random initialization, for each dataset. This is different from the procedure followed for DBNs where each DBN was trained starting from the parameters estimated on the narrower dataset.

of the latent representation with  $n = 12$  variables from  $p^*$ , as a function of depth  $L$  for different datasets, and it shows that the latent space representation approaches  $p^*$  both as depth and as breadth increase. This occurs, for each depth  $L$ , when the dataset (■) containing only the digit ‘2’ of MNIST is expanded to contain translations and rotations of the digit ‘2’ (□), and when it is expanded to contain all the digits in MNIST (▼), then all the characters in EMNIST (▲), and finally when Fashion MNIST is further added to EMNIST (●).

It is also interesting to observe that the estimated values of  $g$  approach the critical point  $g_c = \log 2$  both as depth and as breadth increase (see inset of Fig. 4 b). For  $g = g_c$  the distribution  $p^*$  coincides with a uniform distribution<sup>17</sup>. Yet the representation in the latent space is very different from a uniform distribution. Fig. 4 c) shows that the ten most frequent states of the latent variables (after the transformations of Sect. 4.1) for the AE with  $L = 6$  trained on the broadest dataset (FEM) coincide with the ten most probable states of  $p^*$ . This similarity holds also for other values of  $L$  and datasets.

## 5 Discussion

The main original contribution of this paper is to argue that, in layered information-processing systems such as artificial neural networks and the brain, universal representations emerge spontaneously from the combined effects of depth and breadth. We derive such universal, abstract representation as a fixed point of a RG transformation and we present numerical experiments corroborating this picture.

Abstraction is typically defined in relative terms, depending on what details are considered relevant. The process of abstraction connects different levels of detail in a hierarchy of representations. This process, we argue, can be described by an RG procedure that allows us to define *absolute abstraction* as the fixed point of the RG transformation, which describes the ultimate result of this process, in the limits of infinite detail or infinite generality. The distance from this limit allows us to define a quantitative measure of the level of abstraction of a representation as the Kullback-Leibler distance from the fixed point.

The fact that optimal representations of data rely on universal distributions is a well known fact in source coding. In fact, compression algorithms translate complex datasets into random strings of zeros and ones of maximal entropy [54]. This is also true of generative models such as Variational Auto-encoders [55] and Diffusion Models [56], that map the data to vectors of variables with a preassigned distribution. In these cases, as in source coding, information on the specific nature of the data is stored in the parameters that govern how the data is transformed. For example, in a neural network, the parameters of the different layers capture how each state of a deep representation is dressed by features at different scales, in order to generate data points. The internal representation – the code – just

---

<sup>17</sup>Fitting the internal representations of AEs with the HFM  $h_n$  yields values of  $g$  which are in the range  $[0.15, 0.5]$  for  $L \geq 4$ . These plots show a similar behaviour to that in Fig. 4.

describes how the data is organized, and it is universal because it is the solution of an information theoretic optimization principle. In fact, the only common characteristic of data coming from very different domains is the coding cost, i.e. the number of bits needed to efficiently code each data point. The principle of maximal relevance [10] predicates that the coding cost should be as broadly distributed as possible, which in turn facilitates a robust alignment of different data sources along this dimension. The HFM arises as the ideal abstract representation because it satisfies the principle of maximal relevance, which qualifies it as an optimal scaffold for organizing data according to their coding cost<sup>18</sup>.

This perspective makes the difference between fitting – i.e. estimating the parameters that reproduce the data – and learning – i.e. describing the variation of the data – clear. In addition, integrating data into a pre-existent representations makes learning more similar to understanding, and it endows it with desirable properties for intelligent behaviour<sup>19</sup>, as suggested in Ref. [41]. In fact, the capacity of abstraction is a key ingredient of intelligent behaviour. Abstract representations provide the map of the universe of possibilities that intelligence can navigate to ”handle entirely new tasks that only share abstract commonalities with previously encountered situations.” [58].

The archetypal example of an abstract representation is language. In its general traits, the perspective drawn here resonates with the Chomskyan approach to linguistics, which has been very influential. According to Chomsky [59], one has to distinguish a deep structure – that encodes abstract semantic structures as well as grammatical rules – and a surface structure which is derived from the deep one through a series of transformations leading to the actual, observable form of language as it is spoken or written. The deep structure entails an innate generative process – the *universal grammar* – which is argued to be common to all human languages, and which relies on the capacity of infinite recursion [60] thus making it possible to generate an infinite variety of sentences with a finite vocabulary. The fact that this capacity emerges in children without exposure to much data (spoken language) [61] has led to the hypothesis that universal grammars need to be biologically hardwired, an hypothesis that is not widely accepted [62]. It is tempting to speculate that universal grammars could emerge in deep cortical areas as fixed points of a transformation such as the one discussed here, driven by the integration of inputs from a broad set of sources, across all sensory modalities. Such universal representations would then be shaped by data which is not limited to language. In this view, it would be the integration of all experience into the same framework – that one may call understanding – that promotes abstraction, with the emergence of universal representations.

Understanding how the conceptual framework developed here can be extended to more complex domains such as language is an interesting avenue of further research<sup>20</sup>. In this

---

<sup>18</sup>Note that, in the HFM, the coding cost  $-\log h_n(\mathbf{s}) = gm_{\mathbf{s}} - \log Z_n$  depends linearly on the sufficient statistics  $m_{\mathbf{s}}$ . So the coding cost is itself a sufficient statistics.

<sup>19</sup>At the same time, constraining the internal representation to a data-independent, preassigned model facilitates learning [55] and promotes interpretability [57].

<sup>20</sup>In this respect, we note that the HFM can easily be generalised to variables  $x_i$  taking value in an

paper we confine ourselves to the admittedly oversimplified domain of static representations of binary variables. Also, the range of breadth of the data that our numerical experiments explore is rather limited, as well as the representation capacity of the neural networks analysed. Yet, these results align with empirical studies of large neural networks trained on heterogeneous datasets which exhibit a convergence toward shared representations [6]. This suggests that the RG approach discussed here may be extended to more complex data structures.

## 6 Acknowledgements

We are grateful to Paolo Muratore and Davide Zoccolan for interesting discussions and to Giulia Betelli for her contribution [63]. We acknowledge Max Planck Research School (IMPRS) for The Mechanisms of Mental Function and Dysfunction (MMFD) for supporting Elias Seiffert.

## A Background

In this Section we review theoretical concepts mentioned in the main paper.

### A.1 The relevance

This Section recalls the definition of the relevance. We refer to Ref. [10] for a more extended treatment. We describe representations  $p(\mathbf{s})$  in terms of the variable  $E_{\mathbf{s}} = -\log_2 p(\mathbf{s})$ , which is the minimal number of bits needed to represent state  $\mathbf{s}$ . The average coding cost  $H[\mathbf{s}] = \mathbb{E}[E_{\mathbf{s}}]$  is the usual Shannon entropy and counts the number of bits needed to describe one point of the dataset. Following Ref. [10], we shall call  $H[\mathbf{s}]$  the *resolution*.

The resolution  $H[\mathbf{s}]$  is a measure of information content but not of information “quality”. Meaningful information should bear statistical signatures that allow it to be distinguished from noise. These make it possible to identify relevant information *before* finding out what that information is relevant for, a key feature of learning in living systems. Following Ref. [10], we take the view that the hallmark of meaningful information is a broad distribution of coding costs. Here breadth can be quantified by the *relevance*, which is the entropy of the coding cost  $E_{\mathbf{s}}$

$$H[E] = - \sum_E p(E) \log_2 p(E), \quad (21)$$

---

arbitrary set  $\chi$  by invoking a transformation  $\sigma : \chi \rightarrow \{0, 1\}$  that maps each value of  $x_i$  into a binary variable  $s_i = \sigma(x_i)$  [63]. Extending this analysis in the time dependent domain constitutes a considerably more challenging avenue.

where  $p(E) = W(E)2^{-E}$  is the probability that a state  $\mathbf{s}$  randomly drawn from  $p(\mathbf{s})$  has  $E_{\mathbf{s}} = E$ , and  $W(E)$  is the number of states  $\mathbf{s}$  with  $E_{\mathbf{s}} = E$ . The *principle of maximal relevance* [10] postulates that maximally informative representations should achieve a maximal value of  $H[E]$ , which correspond to a uniform distribution of coding costs ( $p(E) = \text{const}$  or  $W(E) = W_0 2^E$ ). Representations where coding costs are distributed uniformly should be promoted for the reason that, in an optimal representation, the number  $W(E)$  of states  $\mathbf{s}$  that require  $E$  bits to be represented should match as closely as possible the number ( $2^E$ ) of codewords that can be described by  $E$  bits. Representation of maximal relevance with a given resolution also have an exponential degeneracy of states  $W(E) = W_0 e^{\nu E}$ , with  $\nu$  that depends on  $H[\mathbf{s}]$ . Note that states  $\mathbf{s}$  and  $\mathbf{s}'$  with very different coding costs  $E_{\mathbf{s}}$  and  $E_{\mathbf{s}'}$  can be distinguished by their statistics, because they would naturally belong to different typical sets<sup>21</sup>. Representations that maximize the relevance harvest this benefit in discrimination ability that is accorded by statistics alone.

## A.2 The Hierarchical Feature Model

The HFM was introduced in [7], to which we refer for a more complete treatment. The HFM encodes the principle of maximal relevance. It describes the distribution of a string  $\mathbf{s}_{1:n} = (s_1, \dots, s_n)$  of binary variables that we take as indicators of whether each of  $n$  features is present ( $s_i = 1$ ) or not ( $s_i = 0$ ). Features are organised in a hierarchical scale of detail and we require that the occurrence of a feature  $s_k = 1$  at level  $k$  does not provide any information on whether lower order features are present or not. This means that, conditional on  $s_k = 1$ , all lower order features are as random as possible, i.e.  $H[\mathbf{s}_{1:k-1} | s_k = 1] = k - 1$  in bits. This requirement implies that the Hamiltonian  $E_{\mathbf{s}}$  should be a function of  $m_{\mathbf{s}} = \max\{k : s_k = 1\}$ , with  $m_{\mathbf{s}} = 0$  if  $\mathbf{s} = \mathbf{0}$  is the featureless state<sup>22</sup> ( $s_i = 0 \forall i$ ). Since there are  $2^{k-1}$  states with  $m_{\mathbf{s}} = k$ , the principle of maximal relevance (i.e. the requirement that  $W(E) = W_0 e^{\nu E}$ ) excludes all functional forms between  $E_{\mathbf{s}}$  and  $m_{\mathbf{s}}$  that are not linear. This leads to the HFM, that assigns a probability

$$h_n(\mathbf{s}) = \frac{1}{Z_n} e^{-g m_{\mathbf{s}}}, \quad (22)$$

to state  $\mathbf{s}$ , where the partition function  $Z_n$  ensures normalisation. We refer to [7] for a detailed discussion of the properties of the HFM. In brief, in the limit  $n \rightarrow \infty$  the HFM features a phase transition at  $g_c = \log 2$  between a random phase where  $H[\mathbf{s}]$  is of order  $n$  for  $g < g_c$ , and a “low temperature” phase where  $h_n(\mathbf{s})$  is dominated by a finite number of states (and  $H[\mathbf{s}]$  is finite in the limit  $n \rightarrow \infty$ ).

<sup>21</sup>By the law of large numbers, typical samples of weakly interacting variables all have approximately the same coding cost, a fact known as the asymptotic equipartition property [54]. As in Ref. [64], we take the view that a trained neural network distinguishes the points in a dataset in different typical sets.

<sup>22</sup>This is because  $p(\mathbf{s} | m_{\mathbf{s}} = k) = 2^{-k+1}$  so that  $p(\mathbf{s}) = p(\mathbf{s} | m_{\mathbf{s}}) p(m_{\mathbf{s}}) = p(m_{\mathbf{s}}) / 2^{m_{\mathbf{s}}-1}$ .

Marginalising over the low order features  $\mathbf{s}_{1:k}$  returns a mixture between a HFM over the remaining  $n - k$  features and a frozen state

$$\sum_{\mathbf{s}_{1:k}} h_n(\mathbf{s}_{1:n}) = \frac{\xi^k Z_{n-k}}{Z_n} h_{n-k}(\mathbf{s}_{k+1:n}) + \frac{(1 - \xi/2)(\xi^k - 1)}{(\xi - 1)Z_n} \delta_{\mathbf{s}_{k+1:n}, \mathbf{0}_{k+1:n}}. \quad (23)$$

On the other hand, marginalising over the high order ones yields a mixture between the HFM and the uniform (maximum entropy) distribution

$$\sum_{\mathbf{s}_{k+1:n}} h_n(\mathbf{s}_{1:n}) = \frac{Z_k}{Z_n} h_k(\mathbf{s}_{1:k}) + \left(1 - \frac{Z_k}{Z_n}\right) 2^{-k}. \quad (24)$$

## B Details of analytical calculations

In this Section we provide details for the derivations in the theoretical part of the main paper.

### B.1 Existence and uniqueness of the solution for $\alpha$

Each step in the coarse graining RG involves a change in entropy  $\Delta_{k \rightarrow k+1} H = H_{k+1}[s] - H_k[s]$  as follows:

$$\Delta_{1 \rightarrow 2} H = H[s_{1:n-1}] - H[s_{1:n}] = -H[s_n | s_{1:n-1}] \quad (25)$$

$$\Delta_{2 \rightarrow 3} H = H[s_0, s_{1:n-1}] - H[s_{1:n}] = 1 \quad (\text{bits}) \quad (26)$$

$$\Delta_{3 \rightarrow 4} H = h(q) - \alpha H[s_{1:n}] - (1 - \alpha)h(\tilde{p}_n(0_{1:n})), \quad q = \alpha + (1 - \alpha)\tilde{p}_n(0_{1:n}) \quad (27)$$

where  $h(x) = -x \log_2 x - (1 - x) \log_2 (1 - x)$ . Overall the change in entropy is

$$\Delta_{1 \rightarrow 4} H = h(q) - \alpha H[s_{1:n}] - (1 - \alpha)h(\tilde{p}_n(0_{1:n})) + 1 - H[s_n | s_{1:n-1}] \quad (28)$$

therefore  $\alpha$  is the solution of the equation  $\Delta_{1 \rightarrow 4} H = 0$ . Notice that  $\Delta_{1 \rightarrow 4} H(\alpha = 0) \geq 0$  and

$$\frac{d}{d\alpha} \Delta_{1 \rightarrow 4} H = (1 - \tilde{p}_n(0_{1:n})) \log \frac{1 - q}{q} - H[s_n | s_{1:n-1}] + h(\tilde{p}_n(0_{1:n})) \quad (29)$$

which is negative at  $\alpha = 0$  and

$$\frac{d^2}{d\alpha^2} \Delta_{1 \rightarrow 4} H = -\frac{1 - \tilde{p}_n(0_{1:n})}{q(1 - q)} < 0 \quad (30)$$

which means that the solution is unique provided that  $\Delta_{1 \rightarrow 4} H(\alpha = 1) = -H[s_{1:n}] + 1 - H[s_n | s_{1:n-1}]$  is negative. A sufficient condition is that  $H[s_{1:n}] > 1$ .

## B.2 Proof of Eq. (9)

Let us first analyse how the HFM transforms under  $\mathfrak{R}_\uparrow$ . Marginalisation on  $s_n$  yields

$$h_n(\mathbf{s}_{1:n-1}) = \sum_{s_n=0,1} h_n(\mathbf{s}_{1:n}) = \frac{Z_{n-1}}{Z_n} h_{n-1}(\mathbf{s}_{1:n-1}) + \frac{1}{Z_n} e^{-gn} \quad (31)$$

Hence

$$\tilde{p}_n(\mathbf{s}'_{1:n}) = \frac{Z_{n-1}}{2Z_n} h_{n-1}(\mathbf{s}'_{2:n}) + \frac{1}{2Z_n} e^{-gn} \quad (32)$$

If  $\mathbf{s}'_{2:n} = \mathbf{0}$  then

$$h_{n-1}(\mathbf{s}'_{2:n}) = \frac{Z_n}{Z_{n-1}} h_n(\mathbf{s}'_{1:n}) e^{gs'_1} = \frac{Z_n}{Z_{n-1}} h_n(\mathbf{s}'_{1:n}) \left[ e^g + (1 - e^g) \delta_{s'_1,0} \right]$$

because  $m_{\mathbf{s}_{1:n}} = s_1$  in this case. If  $\mathbf{s}'_{2:n} \neq \mathbf{0}_{2:n}$  instead

$$h_{n-1}(\mathbf{s}'_{2:n}) = \frac{Z_n}{Z_{n-1}} e^g h_n(\mathbf{s}'_{1:n})$$

because  $m_{\mathbf{s}_{2:n}} = m_{\mathbf{s}_{1:n}} - 1$ . Therefore, both cases are accounted for by the equation

$$h_{n-1}(\mathbf{s}'_{2:n}) = \frac{Z_n}{Z_{n-1}} e^g h_n(\mathbf{s}'_{1:n}) + \frac{1 - e^g}{Z_{n-1}} \delta_{\mathbf{s}'_{1:n},0} \quad (33)$$

Substituting this into Eq. (32) yields

$$\tilde{p}(\mathbf{s}'_{1:n}) = \frac{e^g}{2} h_n(\mathbf{s}'_{1:n}) + \frac{1 - e^g}{2Z_n} \delta_{\mathbf{s}'_{1:n},0} + \frac{e^{-gn}}{2Z_n} \quad (34)$$

and

$$p'_n(\mathbf{s}'_{1:n}) = (1 - \alpha) \frac{e^g}{2} h_n(\mathbf{s}'_{1:n}) + \left[ \alpha - (1 - \alpha) \frac{e^g - 1}{2Z_n} \right] \delta_{\mathbf{s}'_{1:n},0} + (1 - \alpha) \frac{e^{-gn}}{2Z_n} \quad (35)$$

Therefore, at least for finite  $n$ , the HFM is not a fixed point.

We look for a fixed point of the form

$$p_n^*(s_{1:n}) = (1 - \beta) h_n(s_{1:n}) + \beta u_n(s_{1:n}) \quad (36)$$

exploiting the fact that  $\mathfrak{R}_\uparrow$  is a linear transformation. The uniform distribution  $u_n(s_{1:n}) = 2^{-n}$  transforms as  $\mathfrak{R}_\uparrow(u_n)(\mathbf{s}_{1:n}) = (1 - \alpha) 2^{-n} + \alpha \delta_{\mathbf{s}_{1:n},0}$ .

After some calculation, with  $\xi = 2e^{-g}$ , we find

$$p'_n(\mathbf{s}'_{1:n}) = \frac{(1 - \beta)(1 - \alpha)}{\xi} h_n(\mathbf{s}'_{1:n}) \quad (37)$$

$$+ \left[ (1 - \beta) \left( \alpha - (1 - \alpha) \frac{2 - \xi}{2\xi Z_n} \right) + \beta \alpha \right] \delta_{\mathbf{s}'_{1:n},0} \quad (38)$$

$$+ \left[ \frac{(1 - \beta)(1 - \alpha)}{2Z_n} \xi^n + \beta(1 - \alpha) \right] u_n(\mathbf{s}'_{1:n}) \quad (39)$$

Setting the coefficient of  $h_n(s'_{1:n})$  in the first line (37) to  $1 - \beta$  and the coefficient of  $u_n(s'_{1:n})$  in the third line (39) equal to  $\beta$  yields

$$\alpha = 1 - \xi, \quad \beta = \frac{\xi^{n+1}}{2 - \xi} \quad (40)$$

the second line (38) then vanishes by normalization. The solution then reads

$$p_n^*(\mathbf{s}_{1:n}) = \left(1 - \frac{1}{e^g - 1}\right) e^{-gm_{\mathbf{s}_{1:n}}} + \frac{1}{e^g - 1} e^{-gn}. \quad (41)$$

Interestingly, a solution only exists for  $\xi < 1$ , i.e. for  $g > g_c$ , and in the limit  $g \rightarrow g_c$  the fixed point distribution tends to  $u_n$ . Eq. (41) has the same form of an HFM with  $m > n$  features, marginalised over the  $m - n$  most detailed ones (see Eq. 24). The value of  $m$  can be computed equating  $1 - \beta$  to the coefficient of  $u_n$  in the marginal of  $h_m(\mathbf{s}_{1:m})$  over  $\mathbf{s}_{1:n}$ . This yields the equation

$$\frac{\xi^{m+1}(2 - \xi - \xi^{n+1})}{(2 - \xi)(2 - \xi - \xi^{m+1})} = 0 \quad (42)$$

whose only solution for  $\xi < 1$  is  $m = +\infty$ . In other words, the fixed point  $p_n^*$  is the marginal distribution of the  $n$  most coarse grained features of an HFM with infinite features, which is Eq. (9).

## C Data and deep neural networks

This Section describes first the data used in this study and then the architectures that have been trained on them.

### C.1 Data

We used four standard image datasets: MNIST [65], EMNIST letters [66], Fashion-MNIST [67], and CIFAR-10 [68] downloaded via the torchvision library [69]. Every dataset was binarized before training DBNs (not for auto-encoders) with the following procedure: For MNIST, EMNIST Letters, and FMNIST (all  $28 \times 28$  grayscale), we thresholded pixel intensities at 0.5 to map inputs to  $\{0,1\}$ . For CIFAR-10 (originally  $32 \times 32$  RGB), each image was first converted to grayscale and then binarized with the same threshold then reduced to  $28 \times 28$  via a centered crop that removes a 2-pixel border on each side.

Below we report each dataset’s sizes and concise descriptions:

MNIST: 60 000 handwritten digits (10 classes,  $28 \times 28$ );

EMNIST Letters: 124 800 handwritten letters (26 classes,  $28 \times 28$ ; upper/lowercase merged);

Fashion-MNIST: 60 000 clothing items (10 classes,  $28 \times 28$ );

CIFAR-10: 50 000 natural images (10 classes, originally  $32 \times 32$  RGB).

For sequential DBN training, we constructed datasets of increasing breadth as follows: we first partitioned MNIST into six label sets containing  $\{1, 2, 4, 6, 8, 10\}$  digit classes; we then augmented with EMNIST Letters in three steps: (i) letters a–i, (ii) letters l–r, and (iii) the remaining letters, followed by Fashion-MNIST and, finally, CIFAR-10.

## C.2 DBNs and training procedure

A deep belief networks (DBN) consists of Restricted Boltzmann Machines (RBM) stacked one on top of the other, as shown in Fig.5. Each RBM is a Markov random field with pairwise interactions defined on a bipartite graph of two non interacting layers of variables: visible variables  $\mathbf{x} = (x_1, \dots, x_m)$  representing the data, and hidden variables  $\mathbf{s} = (s_1, \dots, s_n)$  that are the latent representation of the data. The probability distribution of a single RBM is:

$$p(\mathbf{x}, \mathbf{s}) = \frac{1}{Z} \exp \left( \sum_{i,j} W_{ij} x_i s_j + \sum_k x_k c_k + \sum_l s_l b_l \right). \quad (43)$$

where  $\mathbf{W} = \{W_{ij}\}$ ,  $\mathbf{c} = (c_1, \dots, c_m)$  and  $\mathbf{b} = (b_1, \dots, b_n)$  are the parameters that are learned during training.

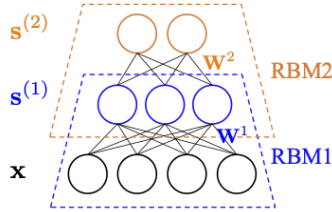


Figure 5: A three layer Deep Belief Network

In order to generate samples from the trained DBN we consider the connections between the top two layers as undirected, whereas all lower layers are connected to the upper layer by directed connections. This means that, in order to obtain a sample from a DBN we initialized a random configuration  $\hat{\mathbf{s}}_0^\ell$ , and performed alternating Gibbs sampling for  $10^6$  steps to ensure convergence to the equilibrium distribution of the top RBM  $p_L(\mathbf{s}^{(L)}, \mathbf{s}^{(L-1)})$ . Then we use this data to sample the states of lower layers using the conditional distribution  $p(\mathbf{s}_{\ell-1} | \mathbf{s}_\ell)$ . In this way, we propagate the signal till the visible layer.

The DBN used in our experiment is the same as that used in Ref. [11]: it has a visible layer with 784 nodes and  $L = 10$  hidden layers with the following number of nodes:  $n_\ell = 500, 250, 120, 60, 30, 25, 20, 15, 10$  and 5, for  $\ell = 1, \dots, 10$ .

We train the DBN one layer at a time, following Hinton’s prescription [45]. First, the bottom RBM is fitted to the data; the dataset  $\hat{\mathbf{x}} = (\mathbf{x}_1, \dots, \mathbf{x}_N)$  is then propagated to the first hidden layer to obtain samples  $\hat{\mathbf{s}}^{(1)}$ , which become the training set for the next RBM.

This type of training procedure was proven [45] to increase a variational lower bound for the log-likelihood.

For each RBM, parameters are learned by stochastic gradient ascent on the log-likelihood, using Persistent Contrastive Divergence with  $k = 10$  (PCD-10), a learning rate of 0.01, and mini-batches of size 100 (see [70]), for  $\sim 10^5$  epochs. With these settings the training of the DBNs does not exhibit mode collapse, which typically occurs when the dataset is strongly clustered and the persistent Markov chain fails to properly mix across all clusters.

We trained the DBN sequentially on datasets of progressively increasing breadth (see Data C.1). At each stage, we restarted training with the same settings (PCD-10, learning rate, mini-batch size, number of epochs), initializing all weights with those learned at the previous stage; we then trained the entire DBN on the extended dataset.

Decelle et al. [52] [71] showed that an RBM trained with CD-10 does not reproduce the equilibrium distribution, yet it can still serve as a good generative model when sampled out of equilibrium. Instead, persistent contrastive divergence (PCD-10), which we use, tends to learn a better equilibrium distribution.<sup>23</sup>

### C.3 Autoencoder Architecture and Training Procedure

The autoencoders employed in this study were trained on the MNIST dataset and its variants [72]. Consequently, all models described below accept an input vector of dimension 784.

#### C.3.1 Architecture

Each model implements a fully connected, feed-forward autoencoder composed of two principal components: an *encoder* that maps the high-dimensional input into a compact latent representation, and a *decoder* that attempts to reconstruct the original input from that representation. The encoder and decoder are constructed symmetrically around a central *bottleneck* (latent) layer, so that the decoder mirrors the encoder’s layer sizes and activation choices in reverse (see Fig. 4 **a**). This symmetric design facilitates interpretation of the learned mapping between input space and latent space and is a common architectural choice for classical autoencoders [46].

The number of hidden layers explored across experiments ranges from one to seven. Let  $n_0 = 784$  denote the input dimension and let  $n_i$  denote the number of neurons in the  $i$ -th hidden layer of the encoder. Successive encoder layers are defined by a fixed geometric reduction factor of 0.6; specifically,

$$n_{i+1} = \lceil 0.6 n_i \rceil,$$

---

<sup>23</sup>In Contrastive Divergence- $k$  (CD- $k$ ), the Markov chain used to sample the distribution is initialized on the batch used to compute the gradient and  $k$  Monte Carlo steps are performed. In Persistent Contrastive Divergence- $k$  (PCD- $k$ ) the MCMC is initialized in the configuration of the previous epoch.

where  $\lceil \cdot \rceil$  denotes the ceiling function to ensure that layer sizes are integer-valued. This progressive compression produces a sequence of hidden sizes that decreases smoothly from the input dimension down to the pre-specified bottleneck dimensionality and provides a controlled way to vary model capacity and depth while keeping the reduction schedule consistent across models.

Activation functions were assigned as follows: all intermediate hidden layers employ the rectified linear unit (ReLU) nonlinearity, defined as  $\text{ReLU}(x) = \max(0, x)$ ; ReLU units are widely used owing to their favorable optimization properties (reduced saturation and mitigated vanishing gradients) [73]. Both the layer immediately preceding the bottleneck and the last layer of the decoder use a sigmoid activation  $\sigma(x) = (1 + e^{-x})^{-1}$ . Attempts of using as output layer the linear function were made, but the networks showed a preference for memorizing datapoints instead of detecting features. Moreover, the Mean Squared Error (see C.3.2) is sensibly lower and better behaved in the case of the sigmoid function as output (see Fig. 6). The latent (bottleneck) dimension itself was treated as a variable: distinct networks were trained with latent dimensions  $d = 10$  and  $12$  in order to study the effect of representational capacity on reconstruction quality and on the geometry of learned codes.

The decoder is symmetric to the encoder: starting from the latent layer, successive layers increase dimensionality according to the inverse schedule (mirroring the reduction factor of the encoder) until the reconstructed output of dimension 784 is produced.

A symmetric architecture reduces the number of arbitrary design choices and often yields decoder features that are naturally aligned with encoder features, easing interpretability of the coding/decoding mapping. In classical autoencoders one can choose to tie decoder weights to the transpose of encoder weights (reducing parameter count and imposing linear symmetry) or allow untied weights (more flexibility at the cost of more parameters). The present work uses untied weights, which provides additional decoder capacity and avoids forcing a linear transpose constraint; the choice was motivated by the aim of assessing how representational dimensionality (bottleneck size) and depth affect reconstruction independent of a tied-weight regularization.

### C.3.2 Training procedure

All networks were trained using the Adam optimizer with learning rate  $\eta = 10^{-3}$  and  $L_2$  weight decay (also referred to as *weight decay*) set to  $10^{-5}$ . Adam is an adaptive first-order optimizer that computes individual learning rates for each parameter from estimates of first and second moments of the gradients and is well suited for stochastic optimization problems that are nonstationary and noisy [74]. The training objective used for all runs was the mean squared error between the input  $x$  and its reconstruction  $\hat{x}$ :

$$\mathcal{L}_{\text{MSE}}(x, \hat{x}) = \frac{1}{D} \sum_{j=1}^D (x_j - \hat{x}_j)^2,$$

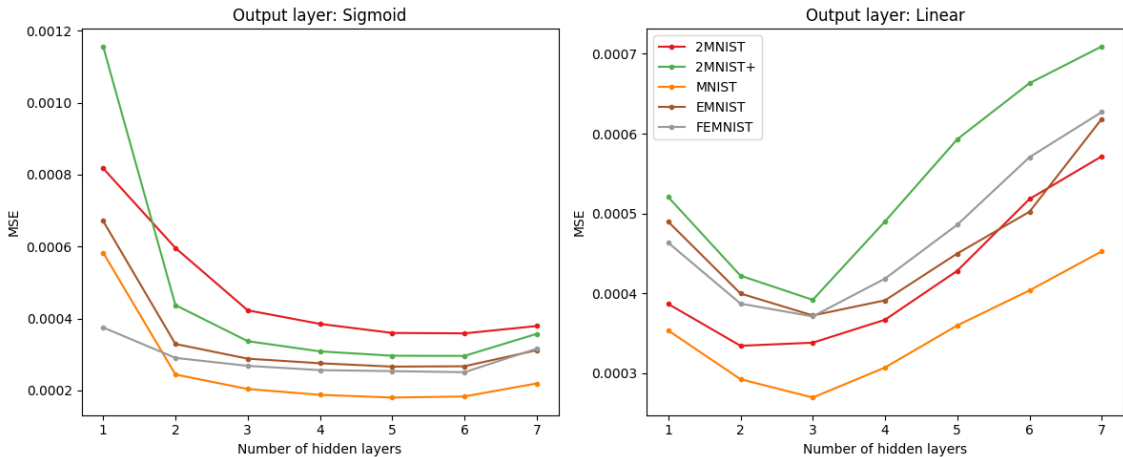


Figure 6: The Mean Squared Error of the autoencoders networks with ten latent dimensions, for the case of sigmoid as output layer (left) and the case of a linear layer (right). In the latter case, the increase of the error for networks with more than three hidden layers coincides with the preference of the network for memorizing data points, rather than detecting features.

where  $D = 784$  is the input dimensionality. MSE is a natural choice when the goal is to minimize Euclidean reconstruction error; for image data preprocessed to lie in  $[0, 1]$ , MSE provides a direct measure of pixelwise fidelity. Each architecture/latent dimension configuration was trained for 10 epochs through the training set.

**Layer-wise pretraining and initialization strategy** To improve optimization stability and to provide favorable initializations for deeper models, a greedy layer-wise pretraining procedure was employed. The pretraining approach used here follows the pragmatic spirit of early deep representation learning strategies in which layers are learned progressively and representations learned by shallower architectures are used to initialize deeper ones [46, 75]... The precise procedure implemented is as follows:

1. Train a shallow autoencoder with a small number of hidden layers (for instance, one hidden layer plus a bottleneck). Training at this stage optimizes the MSE objective for the shallow architecture starting from standard random initialization.
2. When the shallow model has converged, retain the learned weights for the encoder part up to the deepest layer of that shallow model.
3. Construct a deeper model with one additional hidden layer. Initialize the weights of the new deeper model as follows: (i) copy the encoder weights from the previously

trained shallow model into the corresponding positions in the deeper model; (ii) initialize the newly added layers (both encoder and matching decoder layers) with random weights (e.g., small Gaussian i.i.d. initialization); (iii) mirror the copied encoder initializations into the corresponding decoder positions if using symmetric initialization heuristics.

4. Train the deeper model on the same reconstruction objective until convergence.
5. Repeat the expansion and initialization procedure iteratively until the target depth (up to seven hidden layers in this study) is reached.

This greedy scheme yields an initialization for each deeper architecture from parameters that have already learned useful lower-level features; empirically, such initialization can reduce the likelihood of becoming trapped in poor local minima and can accelerate convergence relative to training the deepest architecture from random initialization [46, 75].

**Regularization and normalization** Batch normalization and dropout were intentionally omitted in order to maintain full transparency of the learned latent representations and to avoid introducing additional mechanisms that could obscure the relationship between architecture depth, bottleneck dimensionality, and reconstruction characteristics. Batch normalization can significantly alter the distribution of activations during training and often improves optimization speed and stability [76]; dropout randomly zeros activations during training and acts as an implicit model ensemble/regularizer [77]. While both are valuable tools for improving generalization in many supervised and unsupervised contexts, their use would complicate a direct, controlled investigation of how depth and bottleneck size alone influence the autoencoder’s representational geometry.

## References

- [1] Yoshua Bengio, Ian Goodfellow, and Aaron Courville. *Deep learning*, volume 1. MIT press Massachusetts, USA:, 2017.
- [2] David Marr. *Vision: A computational investigation into the human representation and processing of visual information*. MIT press, 2010.
- [3] John Cardy. *Scaling and renormalization in statistical physics*, volume 5. Cambridge university press, 1996.
- [4] Pankaj Mehta and David J Schwab. An exact mapping between the variational renormalization group and deep learning. *arXiv preprint arXiv:1410.3831*, 2014.
- [5] Ellen De Mello Koch, Robert De Mello Koch, and Ling Cheng. Is deep learning a renormalization group flow? *IEEE Access*, 8:106487–106505, 2020.

- [6] Minyoung Huh, Brian Cheung, Tongzhou Wang, and Phillip Isola. Position: The platonic representation hypothesis. In *Forty-first International Conference on Machine Learning*, 2024.
- [7] Rongrong Xie and Matteo Marsili. A simple probabilistic neural network for machine understanding. *Journal of Statistical Mechanics: Theory and Experiment*, 2024(2):023403, 2024.
- [8] M Marsili, I Mastromatteo, and Y Roudi. On sampling and modeling complex systems. *Journal of Statistical Mechanics: Theory and Experiment*, 2013(09):P09003, 2013.
- [9] Horace B Barlow. Unsupervised learning. *Neural computation*, 1(3):295–311, 1989.
- [10] Matteo Marsili and Yasser Roudi. Quantifying relevance in learning and inference. *Physics Reports*, 963:1–43, 2022.
- [11] J Song, M Marsili, and J Jo. Resolution and relevance trade-offs in deep learning. *Journal of Statistical Mechanics: Theory and Experiment*, 2018(12):123406, dec 2018.
- [12] O Duranthon, M Marsili, and R Xie. Maximal relevance and optimal learning machines. *Journal of Statistical Mechanics: Theory and Experiment*, 2021(3):033409, 2021.
- [13] Carlo Orientale Caputo. Plasticity across neural hierarchies in artificial neural network. Master’s thesis, Politecnico di Torino, Torino, Italy, 2023.
- [14] David H Hubel and Torsten N Wiesel. Receptive fields, binocular interaction and functional architecture in the cat’s visual cortex. *The Journal of physiology*, 160(1):106, 1962.
- [15] Patrice Y Simard, Yann A LeCun, John S Denker, and Bernard Victorri. Transformation invariance in pattern recognition—tangent distance and tangent propagation. In *Neural networks: tricks of the trade*, pages 239–274. Springer, 2002.
- [16] Alessandro Ingrosso and Sebastian Goldt. Data-driven emergence of convolutional structure in neural networks. *Proceedings of the National Academy of Sciences*, 119(40):e2201854119, 2022.
- [17] James J DiCarlo and David D Cox. Untangling invariant object recognition. *Trends in cognitive sciences*, 11(8):333–341, 2007.
- [18] Davide Zoccolan. Invariant visual object recognition and shape processing in rats. *Behavioural brain research*, 285:10–33, 2015.

- [19] Samuel S Schoenholz, Justin Gilmer, Surya Ganguli, and Jascha Sohl-Dickstein. Deep information propagation. In *International Conference on Learning Representations*, 2017. (arXiv preprint arXiv:1611.01232).
- [20] James CR Whittington, David McCaffary, Jacob JW Bakermans, and Timothy EJ Behrens. How to build a cognitive map. *Nature neuroscience*, 25(10):1257–1272, 2022.
- [21] Joshua B Tenenbaum, Charles Kemp, Thomas L Griffiths, and Noah D Goodman. How to grow a mind: Statistics, structure, and abstraction. *science*, 331(6022):1279–1285, 2011.
- [22] John O’Keefe and Jonathan Dostrovsky. The hippocampus as a spatial map: preliminary evidence from unit activity in the freely-moving rat. *Brain research*, 1971.
- [23] David C Rowland, Yasser Roudi, May-Britt Moser, and Edvard I Moser. Ten years of grid cells. *Annual review of neuroscience*, 39:19–40, 2016.
- [24] Uta Noppeney, Samuel A Jones, Tim Rohe, and Ambra Ferrari. See what you hear—how the brain forms representations across the senses. *Neuroforum*, 24(4):A169–A181, 2018.
- [25] James J DiCarlo, Davide Zoccolan, and Nicole C Rust. How does the brain solve visual object recognition? *Neuron*, 73(3):415–434, 2012.
- [26] Alessio Ansuini, Alessandro Laio, Jakob H Macke, and Davide Zoccolan. Intrinsic dimension of data representations in deep neural networks. In *Advances in Neural Information Processing Systems*, pages 6111–6122, 2019.
- [27] Yuansheng Zhou, Brian H Smith, and Tatyana O Sharpee. Hyperbolic geometry of the olfactory space. *Science advances*, 4(8):eaq1458, 2018.
- [28] Tomaso Poggio, Hrushikesh Mhaskar, Lorenzo Rosasco, Brando Miranda, and Qianli Liao. Why and when can deep-but not shallow-networks avoid the curse of dimensionality: a review. *International Journal of Automation and Computing*, 14(5):503–519, 2017.
- [29] Uri Cohen, SueYeon Chung, Daniel D Lee, and Haim Sompolinsky. Separability and geometry of object manifolds in deep neural networks. *Nature communications*, 11(1):746, 2020.
- [30] Emmanuel Abbe, Enric Boix-Adsera, Matthew S Brennan, Guy Bresler, and Dheeraj Nagaraj. The staircase property: How hierarchical structure can guide deep learning. *Advances in Neural Information Processing Systems*, 34:26989–27002, 2021.

- [31] Emily Cheng, Diego Doimo, Corentin Kervadec, Iuri Macocco, Jade Yu, Alessandro Laio, and Marco Baroni. Emergence of a high-dimensional abstraction phase in language transformers. *arXiv preprint arXiv:2405.15471*, 2024.
- [32] Francesco Cagnetta, Leonardo Petrini, Umberto M Tomasini, Alessandro Favero, and Matthieu Wyart. How deep neural networks learn compositional data: The random hierarchy model. *Physical Review X*, 14(3):031001, 2024.
- [33] Daniel Mirman, Jon-Frederick Landrigan, and Allison E Britt. Taxonomic and thematic semantic systems. *Psychological bulletin*, 143(5):499, 2017.
- [34] Charles P Davis and Eiling Yee. Features, labels, space, and time: Factors supporting taxonomic relationships in the anterior temporal lobe and thematic relationships in the angular gyrus. *Language, Cognition and Neuroscience*, 34(10):1347–1357, 2019.
- [35] Takashi Namba and Wieland B Huttner. What makes us human: insights from the evolution and development of the human neocortex. *Annual review of cell and developmental biology*, 40(1):427–452, 2024.
- [36] Satoshi Iso, Shotaro Shiba, and Sumito Yokoo. Scale-invariant feature extraction of neural network and renormalization group flow. *Phys. Rev. E*, 97:053304, May 2018.
- [37] Dietmar Plenz, Tiago L Ribeiro, Stephanie R Miller, Patrick A Kells, Ali Vakili, and Elliott L Capek. Self-organized criticality in the brain. *arXiv preprint arXiv:2102.09124*, 2021.
- [38] T Mora and W Bialek. Are biological systems poised at criticality? *Journal of Statistical Physics*, 144(2):268–302, 2011.
- [39] G Tkačik, T Mora, O Marre, D Amodei, S E Palmer, M J Berry, and W Bialek. Thermodynamics and signatures of criticality in a network of neurons. *Proceedings of the National Academy of Sciences*, 112(37):11508–11513, 2015.
- [40] Ryan John Cubero, Junghyo Jo, Matteo Marsili, Yasser Roudi, and Juyong Song. Statistical criticality arises in most informative representations. *Journal of Statistical Mechanics: Theory and Experiment*, 2019(6):063402, jun 2019.
- [41] Rongrong Xie and Matteo Marsili. A random energy approach to deep learning. *Journal of Statistical Mechanics: Theory and Experiment*, 2022(7):073404, 2022.
- [42] Martino Sorbaro, J Michael Herrmann, and Matthias Hennig. Statistical models of neural activity, criticality, and zipf’s law. In *The Functional Role of Critical Dynamics in Neural Systems*, pages 265–287. Springer, 2019.
- [43] Alexandre Pouget, Peter Dayan, and Richard Zemel. Information processing with population codes. *Nature Reviews Neuroscience*, 1(2):125–132, 2000.

- [44] Sebastian Goldt, Marc Mézard, Florent Krzakala, and Lenka Zdeborová. Modeling the influence of data structure on learning in neural networks: The hidden manifold model. *Physical Review X*, 10(4):041044, 2020.
- [45] Geoffrey E Hinton, Simon Osindero, and Yee-Whye Teh. A fast learning algorithm for deep belief nets. *Neural computation*, 18(7):1527–1554, 2006.
- [46] Geoffrey E Hinton and Ruslan R Salakhutdinov. Reducing the dimensionality of data with neural networks. *science*, 313(5786):504–507, 2006.
- [47] Martin R Evans, Satya N Majumdar, and Grégory Schehr. Stochastic resetting and applications. *Journal of Physics A: Mathematical and Theoretical*, 53(19):193001, apr 2020.
- [48] Nicolaas Govert De Bruijn. A combinatorial problem. *Proceedings of the Section of Sciences of the Koninklijke Nederlandse Akademie van Wetenschappen te Amsterdam*, 49(7):758–764, 1946.
- [49] Bas Lemmens and Roger Nussbaum. *Nonlinear Perron-Frobenius Theory*, volume 189. Cambridge University Press, 2012.
- [50] Vriddhachalam K Balasubrahmanyam and Sundaresan Naranan. Algorithmic information, complexity and zipf’s law. *Glottometrics*, 4:1–26, 2002.
- [51] J D Burgos and P Moreno-Tovar. Zipf-scaling behavior in the immune system. *Biosystems*, 39(3):227 – 232, 1996.
- [52] Aurélien Decelle, Cyril Furtlehner, and Beatriz Seoane. Equilibrium and non-equilibrium regimes in the learning of restricted boltzmann machines. *Advances in Neural Information Processing Systems*, 34:5345–5359, 2021.
- [53] Guido Montúfar. Restricted boltzmann machines: Introduction and review. In *Information Geometry and Its Applications IV*, pages 75–115. Springer, 2016.
- [54] T M Cover and J A Thomas. *Elements of information theory*. John Wiley & Sons, 2012.
- [55] Diederik P Kingma and Max Welling. Auto-encoding variational bayes. In *Int. Conf. on Learning Representations (Banff)*, 2014.
- [56] Jascha Sohl-Dickstein, Eric Weiss, Niru Maheswaranathan, and Surya Ganguli. Deep unsupervised learning using nonequilibrium thermodynamics. In *International conference on machine learning*, pages 2256–2265. pmlr, 2015.

- [57] Irina Higgins, Loic Matthey, Arka Pal, Christopher Burgess, Xavier Glorot, Matthew Botvinick, Shakir Mohamed, and Alexander Lerchner. beta-vae: Learning basic visual concepts with a constrained variational framework. In *International conference on learning representations*, 2017.
- [58] François Chollet. On the measure of intelligence. *arXiv preprint arXiv:1911.01547*, 2019.
- [59] Noam Chomsky. *Aspects of the Theory of Syntax*. The MIT Press, Cambridge, MA, 1965.
- [60] Marc D Hauser, Noam Chomsky, and W Tecumseh Fitch. The faculty of language: what is it, who has it, and how did it evolve? *Science*, 298(5598):1569–1579, 2002.
- [61] Steven Pinker. *The language instinct: How the mind creates language*. Penguin uK, 2003.
- [62] Michael Tomasello. *Constructing a language: A usage-based theory of language acquisition*. Harvard university press, 2005.
- [63] Giulia Betelli. Una generalizzazione dello hierarchical feature model. Unpublished bachelor’s thesis, University of Trieste, Trieste, 2024.
- [64] R Shwartz-Ziv and N Tishby. Opening the black box of deep neural networks via information. *arXiv preprint arXiv:1703.00810*, 2017.
- [65] Yann LeCun, Léon Bottou, Yoshua Bengio, and Patrick Haffner. Gradient-based learning applied to document recognition. *Proceedings of the IEEE*, 86(11):2278–2324, 1998.
- [66] Gregory Cohen, Saeed Afshar, Jonathan Tapson, and Andre Van Schaik. Emnist: Extending mnist to handwritten letters. In *2017 international joint conference on neural networks (IJCNN)*, pages 2921–2926. IEEE, 2017.
- [67] Han Xiao, Kashif Rasul, and Roland Vollgraf. Fashion-mnist: a novel image dataset for benchmarking machine learning algorithms, 2017.
- [68] Alex Krizhevsky. Learning multiple layers of features from tiny images. 2009.
- [69] Adam Paszke, Sam Gross, Francisco Massa, Adam Lerer, James Bradbury, Gregory Chanan, Trevor Killeen, Zeming Lin, Natalia Gimelshein, Luca Antiga, Alban Desmaison, Andreas Kopf, Edward Yang, Zachary DeVito, Martin Raison, Alykhan Tejani, Sasank Chilamkurthy, Benoit Steiner, Lu Fang, Junjie Bai, and Soumith Chintala. Pytorch: An imperative style, high-performance deep learning library. In *Advances in Neural Information Processing Systems 32 (NeurIPS)*, pages 8024–8035, 2019.

- [70] Geoffrey E Hinton. A practical guide to training restricted boltzmann machines. In *Neural networks: Tricks of the trade*, pages 599–619. Springer, 2012.
- [71] Elisabeth Agoritsas, Giovanni Catania, Aurélien Decelle, and Beatriz Seoane. Explaining the effects of non-convergent sampling in the training of energy-based models. In *ICML 2023-40th International Conference on Machine Learning*, 2023.
- [72] Yann LeCun. The mnist database of handwritten digits. <http://yann.lecun.com/exdb/mnist/>, 1998.
- [73] Vinod Nair and Geoffrey E. Hinton. Rectified linear units improve restricted boltzmann machines. In *Proceedings of the 27th International Conference on Machine Learning (ICML)*, 2010.
- [74] Diederik P. Kingma and Jimmy Lei Ba. Adam: A Method for Stochastic Optimization. *arXiv preprint arXiv:1412.6980*, 2014.
- [75] Yoshua Bengio, Pascal Lamblin, Dan Popovici, and Hugo Larochelle. Greedy layer-wise training of deep networks. In *Advances in Neural Information Processing Systems (NIPS)*, pages 153–160, 2007.
- [76] Sergey Ioffe and Christian Szegedy. Batch normalization: Accelerating deep network training by reducing internal covariate shift. In *Proceedings of the 32nd International Conference on Machine Learning (ICML)*, 2015.
- [77] Nitish Srivastava, Geoffrey Hinton, Alex Krizhevsky, Ilya Sutskever, and Ruslan Salakhutdinov. Dropout: A simple way to prevent neural networks from overfitting. *Journal of Machine Learning Research*, 15:1929–1958, 2014.